

# Transesterification of palm oil using KF and NaNO<sub>3</sub> catalysts supported on spherical millimetric $\gamma$ -Al<sub>2</sub>O<sub>3</sub>

Aminul Islam<sup>a,b</sup>, Yun Hui Taufiq-Yap<sup>b</sup>, Chi-Ming Chu<sup>a</sup>, Pogaku Ravindra<sup>a</sup>, Eng-Seng Chan<sup>c,\*</sup>

<sup>a</sup> Centre of Materials and Minerals, School of Engineering and IT, Universiti Malaysia Sabah, 88999 Kota Kinabalu, Malaysia

<sup>b</sup> Centre of Excellence for Catalysis Science and Technology, Faculty of Science, University Putra Malaysia, 43400 UPM Serdang, Selangor, Malaysia

<sup>c</sup> School of Engineering, Monash University, Jalan Lagoan Selatan, 46150 Bandar Sunway, Selangor, Malaysia

## ARTICLE INFO

### Article history:

Received 22 May 2012

Accepted 23 January 2013

Available online 12 April 2013

### Keywords:

Gamma-alumina

Transesterification

Biodiesel

Heterogenous catalyst

Potassium fluoride

Sodium nitrate

## ABSTRACT

The use of spherical millimetric gamma-alumina ( $\gamma$ -Al<sub>2</sub>O<sub>3</sub>) as a catalyst support for the production of biodiesel from palm oil is demonstrated. The catalyst support was produced using a dripping method, and KF and NaNO<sub>3</sub> catalysts were loaded on the support using the impregnation method. X-ray diffraction (XRD) analysis showed the formation of Na<sub>2</sub>O and NaAlO<sub>2</sub> phases on the NaNO<sub>3</sub>/ $\gamma$ -Al<sub>2</sub>O<sub>3</sub> catalyst and the formation of K<sub>2</sub>O and KAlF<sub>4</sub> on the KF/ $\gamma$ -Al<sub>2</sub>O<sub>3</sub> catalyst, which were possibly the active sites for the transesterification reaction. The highest number and strength of basic sites generated from the solid phase reaction of the KF/ $\gamma$ -Al<sub>2</sub>O<sub>3</sub> catalyst loaded with 0.24 g KF/g  $\gamma$ -Al<sub>2</sub>O<sub>3</sub> and the NaNO<sub>3</sub>/ $\gamma$ -Al<sub>2</sub>O<sub>3</sub> catalyst loaded with 0.30 g NaNO<sub>3</sub>/g  $\gamma$ -Al<sub>2</sub>O<sub>3</sub> were confirmed by temperature programmed desorption of CO<sub>2</sub> (CO<sub>2</sub>-TPD) analysis. The nitrogen adsorption–desorption isotherms also revealed a mesoporous structure of the catalysts. The biodiesel yield was comparable to that produced from smaller catalysts, and this result indicated the potential of the macrospherical catalysts.

© 2013 Elsevier Ltd. All rights reserved.

## 1. Introduction

There has been an increase in research activity directed toward the development of heterogenous catalysts for the production of biodiesel in a more energy and environmentally friendly way than the conventional homogeneously catalyzed process. Many metal oxides or alkali metals include alkali earth metal and transition metal have been used to catalyze the methanolysis of vegetable oils.

Many works have focused on improving the biodiesel yield by varying the chemical composition and some basic physical properties of the catalyst, as summarized by Zabeti et al. [1]. Among the alumina supported catalysts reported are KI/Al<sub>2</sub>O<sub>3</sub> [2], Mg(NO<sub>3</sub>)<sub>2</sub>/Al<sub>2</sub>O<sub>3</sub> [3], Na/NaOH/ $\gamma$ -Al<sub>2</sub>O<sub>3</sub> [4], NaOH/Al<sub>2</sub>O<sub>3</sub> [5], KNO<sub>3</sub>/Al<sub>2</sub>O<sub>3</sub> [6] and K/KOH/ $\gamma$ -Al<sub>2</sub>O<sub>3</sub> [7]. These catalysts were normally prepared in powdered form (i.e.  $\mu$ m in diameter). Recently, the utilization of Al<sub>2</sub>O<sub>3</sub> support having a particle size of nano-meter order for biodiesel production has been demonstrated [8,9]. The small particle size may offer high catalytic activity but it gives rise

to several problems such as high pressure drops, poor mass/heat transfer, poor contact efficiency and difficulties in separation [10,11]. There are also possible health risks caused by inhalation of small particles. It has been suggested to fabricate the metal oxide catalysts into macroscopic form if they are to be useful for industrial applications [12]. In addition, supported catalyst in spherical form can offer shape-dependent advantages such as minimizing the abrasion of catalyst in the reaction environment as reported by Campanati et al. [13].

Until now, there has been limited work to prepare alkali metal based catalyst in macroscopic form to catalyze the transesterification reaction for biodiesel production. In a recent work, Wang et al. [12] prepared a magnesia-rich magnesium aluminate spinel (MgO·MgAl<sub>2</sub>O<sub>4</sub>) framework catalyst using  $\gamma$ -Al<sub>2</sub>O<sub>3</sub> macro-spheres (up to 1.0 mm in diameter) as a hard template. The process involves in situ growth of an magnesium–aluminum layered double hydroxides (MgAl-LDHs) precursor within the pore channels of the  $\gamma$ -Al<sub>2</sub>O<sub>3</sub> template, followed by spinel formation and the selective removal of the template by leaching with alkali. The catalyst was used for methanolysis of soybean oil and the biodiesel yield was also compared to that produced using MgO/MgAl<sub>2</sub>O<sub>4</sub>/ $\gamma$ -Al<sub>2</sub>O<sub>3</sub> catalyst prepared by conventional impregnation of the  $\gamma$ -Al<sub>2</sub>O<sub>3</sub> spheres with magnesium nitrate solution, followed by drying and

\* Corresponding author. Tel.: +60 3 55145821; fax: +60 3 55146207.

E-mail address: [chan.eng.seng@monash.edu](mailto:chan.eng.seng@monash.edu) (E.-S. Chan).

calcination. However, the biodiesel yield obtained with the catalyst  $\text{MgO} \cdot \text{MgAl}_2\text{O}_4$  and  $\text{MgO}/\text{MgAl}_2\text{O}_4/\gamma\text{-Al}_2\text{O}_3$  were substantially low at 57% and 36% respectively in 10 h.

The aim of this work was to improve the biodiesel yield from transesterification of palm oil using a spherical millimetric gamma-alumina ( $\gamma\text{-Al}_2\text{O}_3$ ) catalyst support.  $\gamma\text{-Al}_2\text{O}_3$  was chosen because it can easily be synthesized, it possesses good support properties, and it is commercially available. Two model catalysts were compared: potassium fluoride (KF) and sodium nitrate ( $\text{NaNO}_3$ ). The catalysts were prepared at different loading contents, and the effects of these catalysts on the transesterification reaction were evaluated in terms of the FAMES yield. In addition, the characteristics of the synthesized catalysts, such as the structural, morphological, textural and base properties, were carried out using X-ray diffraction (XRD), scanning electron microscopy (SEM),  $\text{N}_2$  adsorption/desorption isotherms and  $\text{CO}_2$ -temperature-programmed reduction (TPD) techniques. The relationship between the basicity of the catalyst and their catalytic activity in the transesterification of palm oil is also discussed.

## 2. Experimental

### 2.1. Materials

Boehmite ( $\text{AlOOH}$ ) in a powder form was provided by BASF Catalysis LLC, USA (G-250). Reagents used during catalyst synthesis were: hydrochloric acid (JT Baker Hydrochloric Acid, Model 9530-33, Mexico), ammonia solution (System. ChemAR, Malaysia) and Paraffin oil (Ajax chemicals, 356-2.5L GL, Australia). Commercial edible grade palm oil was purchased from a local store (Lam Soon Malaysia). Methanol (Lab-scan, Thailand) was used for the transesterification reactions and hexane was purchased from Fisher Scientific (Code: 12626717, UK). Methyl heptadecanoate (internal standard for gas chromatography, CAS: 1731-92-6, Switzerland) and standard references such as methyl myristate (Fluka, Ec no. 2046801, Switzerland), Methyl stearate (CAS: 112-61-8, USA), methyl palmitate (Ec No: 2046801), methyl oliate (CAS: 112-62-9, Fluka, USA) and methyl lineate (CAS: 112-61-8, USA) were used for fatty acid methyl ester analysis.

### 2.2. Preparation of catalyst

Spherical millimetric gamma-alumina ( $\gamma\text{-Al}_2\text{O}_3$ ) support was prepared using a sol–gel process previously described by Wang and Lin [14]. In brief, the boehmite powder (300 g/L) was suspended in deionized water and dispersed ultrasonically for 3 min at 70% amplitude. The pH of the boehmite suspension was then adjusted to 1.0 by adding HCl, where the sol turned to a gel. The gel was then transferred dropwise using a pump into a liquid column

consisting of paraffin oil in the upper layer and ammonia solution in the bottom layer. Boehmite gel droplets were formed because of the surface tension effect during transiting through the oil layer, and the gel droplets were aged in the ammonia solution for 1 h. During aging, the ammonia would neutralize the acid in the wet-gel beads, and thus, the wet-gel droplets became rigid. Then, the particles were separated by simple filtration and washed with water. The particles were then dried in air at room temperature (25 °C) for 12 h and were later calcined at 800 °C for 3 h. The calcined  $\gamma\text{-Al}_2\text{O}_3$  particles were then impregnated with an aqueous solution of potassium fluoride (KF) or sodium nitrate ( $\text{NaNO}_3$ ) for an hour. The amount of KI KF and  $\text{NaNO}_3$  impregnation was maintained 0.06, 0.15, 0.24, 0.30 g (catalyst and 0.33 g/g  $\gamma\text{-Al}_2\text{O}_3$ ). The basic principle of impregnation methods is the amount of support is equal to the amount of solution absorbed by the support. The impregnation of catalyst is given in Table 1. Finally, the particle-supported catalysts were calcined at 500 °C for 3 h and used for biodiesel production.

### 2.3. Characterization of catalyst

#### 2.3.1. Shape and size

The size and the shape of the support particles were determined using an image analyzer (Sigma ScanPro 5) (Fig. 1). The particles were viewed under a stereozoom microscope (Stemi DV4, Carl Zeiss, Germany), and their images were taken using a digital camera (Moticam-350, version 2.0 ML, China) attached to the eye piece. The sphericity factor (SF) was used to indicate the roundness of the particles, as described by Chan [15], (where the value zero indicates a perfect sphere and higher values indicate a greater degree of shape distortion). SF was calculated according to eq. (1):

$$\text{SF} = (D_{\text{max}} - D_{\text{per}}) / (D_{\text{max}} + D_{\text{per}}) \quad (1)$$

where  $D_{\text{max}}$  is the maximum diameter passing through a particle centroid (mm), and  $D_{\text{per}}$  is the diameter perpendicular to  $D_{\text{max}}$  passing through the particle centroid (mm).

#### 2.3.2. Structure

The chemical composition of the catalyst was determined using a Shimadzu diffractometer, model XRD-6000. The diffractometer employed Cu–K $\alpha$  radiation to generate diffraction patterns from powder crystalline samples. The Cu–K $\alpha$  radiation was generated with a Philips glass diffraction X-ray tube of the broad focus 2.7 kW type. All samples were mounted on sample holders, and the measurements were performed at  $2\theta$  values between 10 and 70°, with a step size of 0.05° at a speed of 0.05 s<sup>-1</sup>. The data were analyzed with the DiffracPlus software, and the phases were identified using the powder diffraction file (PDF) database (JCPDS, International Centre for Diffraction Data).

**Table 1**  
Impregnation of catalyst.

Step-1	Step-2	Step-3	Step-4	Step-5	Step-6	Step-7
Catalyst (g) for 1 g support	Support (g)	Catalyst (g) for 3 g of support	Volume of aqueous solution (ml) of catalyst impregnated by 3 g of support	Calcination	Total weight of catalyst and support (g)	The calcinated catalyst, g (catalyst + support) used for biodiesel production (4 wt%, g cat./g oil)
0.06	3	3 × 0.06 = 0.18	4.5	Calcination of	3.18	0.6
0.15	3	3 × 0.15 = 0.45	4.5	impregnated catalyst	3.45	0.6
0.24	3	3 × 0.24 = 0.72	4.5		3.72	0.6
0.30	3	3 × 0.30 = 0.90	4.5		3.90	0.6
0.33	3	3 × 0.33 = 0.99	4.5		3.99	0.6

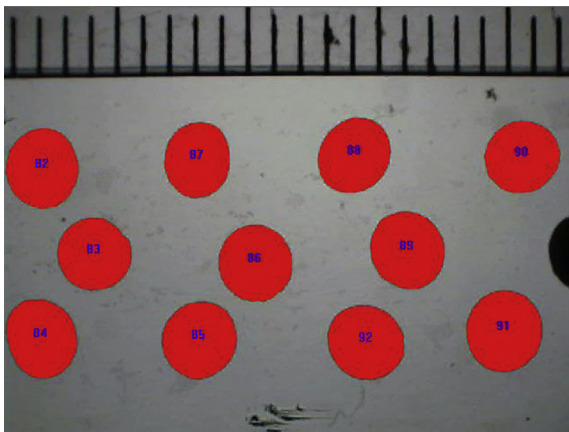


Fig. 1. Particle size and shape measured by image analyzing software.

### 2.3.3. Basicity

The basicity of the catalyst was investigated by the CO<sub>2</sub>-TPD method, using CO<sub>2</sub> as a probe molecule. The TPD-CO<sub>2</sub> experiments were performed using a Thermo Finnigan TPD/R/O 1100 series catalytic surface analyzer equipped with a thermal conductivity detector. Catalysts (100 mg) were pretreated under a helium stream at 800 °C for 30 min (10 °C min<sup>-1</sup>, 30 mL min<sup>-1</sup>). Then, the temperature was decreased to 30 °C with a flow of pure CO<sub>2</sub> (30 mL min<sup>-1</sup>) into the reactor for 1 h. The sample was flushed with helium at 30 °C for 30 min prior to the CO<sub>2</sub> desorption analysis. The analysis of CO<sub>2</sub> desorption was then carried out up to 800 °C under a helium flow (10 °C min<sup>-1</sup>, 30 mL min<sup>-1</sup>), and the amount of desorbed CO<sub>2</sub> was detected and determined using a thermal conductivity detector (TCD).

### 2.3.4. Surface area and pore structure

The surface area, pore volume and pore size of the catalyst were measured from the nitrogen adsorption–desorption isotherms at liquid nitrogen temperature (–196 °C). All of the samples were degassed at 150 °C under vacuum conditions until no pressure gradient could be detected. The analysis was conducted using Thermo Finnigan Sorptomatic 1900 series nitrogen adsorption/desorption analysis software. The total surface area of the catalysts was obtained by the Brunauer, Emmett and Teller (BET) method from the linear part of the nitrogen adsorption isotherms. Total pore volume was calculated according to the Gurvitch method for  $p/p_0 = 0.95$ . The pore size distribution was obtained according to the Barrett, Joyner and Halenda (BJH) method from the desorption branch of the isotherm.

### 2.4. Transesterification reaction conditions

The transesterification reaction was carried out in a 50 mL baffled conical flask (Corning, USA) placed in an incubator orbital shaker equipped with a temperature controller. According to stoichiometry of the transesterification reaction, 3 mol of methanol are required to react with each mole of triglyceride, but in practice a higher molar ratio is employed in order to drive the reaction towards completion and produce more methyl esters as product. The methanol oil ratio of 14 was found to allow the reaction to proceed at a high rate [16]. Hence, the methanol oil molar ratio was kept at 14:1 in this study.

On the other hand, the catalyst concentration reported in the literature was in the range of 4–35 wt% ( $g_{cat}/g_{oil}$ ). The yield of fatty acid alkyl esters generally increases with increasing amount of catalyst. However, the addition of excessive amount of catalyst allowed the formation of emulsion which increased the liquid

viscosity [17]. The high viscosity hindered the glycerol separation and might reduce the ester yield. Therefore, the lowest catalyst concentration, i.e. 4 wt%, was chosen in this study.

The reaction was performed at 60 °C over a period of 4 h. The operating temperature was chosen because it is near to the boiling point of methanol. The reaction mixture was stirred at an agitation speed of 250 rpm to allow good contact between the catalyst and reactants. After the completion of the reaction, the catalyst was separated from the reaction mixture by simple filtration. The filtrate was then centrifuged at a relative centrifugal force of 2500 g for 10 min, and then excessive amount of methanol was evaporated before analysis of biodiesel yield was conducted.

### 2.5. Analysis of biodiesel

The composition of the biodiesel produced was determined using gas chromatography (Shimadzu GC-14B) with a capillary column (30 m × 0.5 mm × 0.25 μm) and flame ionization detector (FID). The injector and detector temperatures were 240 and 280 °C, respectively. The initial oven temperature was 80 °C, with an equilibrium time of 1 min. After the isothermal period, the oven was heated at a rate of 10 °C/min to 270 °C, and the temperature was maintained for 7 min. Hexane was used as a solvent, and methyl heptadecanoate was used as an internal standard. In all, 0.2 g of biodiesel sample was weighed and added to a solution of methyl heptadecanoate at a concentration of 0.1 g per 100 mL of hexane. A total of 0.5 μL of the resulting solution was injected into the gas chromatograph, and helium was used as the carrier gas. The peaks of the methyl esters were identified by comparing them with the respective standards. The content in fatty acid methyl ester (FAME) yield was determined in accordance with European regulated procedure EN 14103 [18]. The results were obtained as an average of duplicate experiments.

To calculate the biodiesel yield, the response factors,  $R_f$  for each compound have been calculated using the correspondent standard compound according to the Eq. (2).

$$R_f = (A_{is}/A_{rs}) \times (C_{rs}/C_{is}) \quad (2)$$

where,  $A_{is}$  = area of internal standard,  $C_{is}$  = concentration of internal standard,  $A_{rs}$  = area of standard references,  $C_{rs}$  = concentration of standard references.

The methyl ester (ME) was calculated using Eq. (3):

$$ME = (C_{iss} \times A_{if} \times R_f) / A_{iss} \quad (3)$$

where,  $C_{iss}$  = concentration of internal standard in the sample,  $A_{iss}$  = area of internal standard in the sample,  $A_{if}$  = area of individual FAMEs compound in the sample. The biodiesel yield (%) was according to the Eq. (4):

$$\text{Biodiesel yield}(\%) = \frac{\text{Total amount of methyl ester}(\text{mol})}{3 \times \text{Charge amount of triglycerols}(\text{mol})} \times 100 \quad (4)$$

## 3. Results and discussion

### 3.1. Size and shape of catalyst

Fig. 2 shows the optical photograph of the millimetric  $\gamma$ -Al<sub>2</sub>O<sub>3</sub> support particles derived from the sol–gel process after calcination. As can be seen, the particles were spherical in shape and had a particle size of 2 mm in diameter. The particles were spherical with

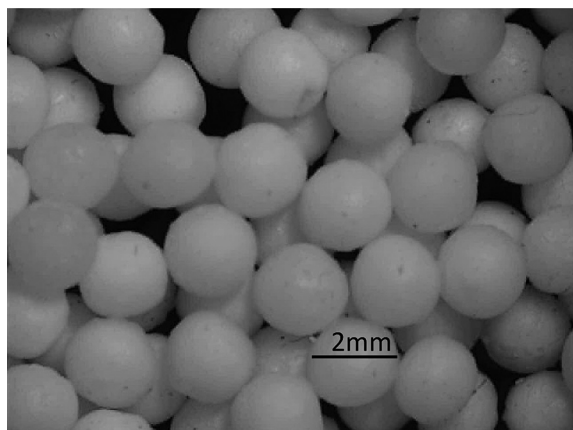


Fig. 2. Optical photograph of the millimetric  $\gamma$ - $\text{Al}_2\text{O}_3$  particles.

a sphericity factor (SF) of  $0.02 \pm 0.01$ . It has been found that a particle can be considered spherical if the spherical factor is less than 0.05 [19].

### 3.2. Structure of catalyst

The XRD patterns of the  $\text{KF}/\gamma\text{-Al}_2\text{O}_3$  catalyst calcined at  $500^\circ\text{C}$  are presented in Fig. 3. As for the KF content of  $0.06\text{ g/g } \gamma\text{-Al}_2\text{O}_3$  (curve a), the characteristics peaks of  $\gamma\text{-Al}_2\text{O}_3$  (JCPDS File No. 00-029-0063) at  $2\theta = 45.79^\circ$  and  $66.76^\circ$ , and KF (JCPDS File No. 00-036-1458) at  $2\theta = 28.89^\circ$  were observed. An additional peak associated with the  $\text{K}_2\text{O}$  phase ( $2\theta = 42.78^\circ$ ) appeared in the diffraction patterns at a loading of  $0.6\text{ g/g } \gamma\text{-Al}_2\text{O}_3$  [8]. As the loading amount of KF was increased to  $0.15\text{ g/g } \gamma\text{-Al}_2\text{O}_3$ , a small increase of the characteristic peaks intensity was observed (curve b). The KF peak could still be detected at a loading below  $0.24\text{ g/g } \gamma\text{-Al}_2\text{O}_3$  although the intensities of these peaks were not as high as those observed for loadings above  $0.24\text{ g/g } \gamma\text{-Al}_2\text{O}_3$ . Based on these results, it was likely that only a part of the loaded KF decomposed under calcination conditions at loadings below  $0.24\text{ g/g } \gamma\text{-Al}_2\text{O}_3$ . These results agree well with the results of  $\text{KI}/\text{Al}_2\text{O}_3$  reported by Xie et al. (2006). They explained that at low KI loading, the XRD patterns were identical to that of KI because of the partial

decomposition of KI on  $\text{Al}_2\text{O}_3$ . The diffraction lines (curve c) assigned to  $\text{K}_2\text{O}$  (JCPDS File No. 00-023-0493) at  $2\theta = 23.88^\circ$  and  $30.0^\circ$ , and  $\text{KAlF}_4$  (JCPDS File No. 00-040-0549) at  $2\theta = 35.52^\circ$  appeared with a KF catalyst loading of  $0.24\text{ g/g } \gamma\text{-Al}_2\text{O}_3$ . The KF phase was undetectable at this loading probably due to its decomposition and interaction with the  $\gamma\text{-Al}_2\text{O}_3$  and formation of new phases of  $\text{K}_2\text{O}$  and  $\text{KAlF}_4$ . At  $0.30\text{ g/g } \gamma\text{-Al}_2\text{O}_3$  (curve d), the KF diffraction line reappeared at  $2\theta = 28.89^\circ$  and the line was more intense when the KF loading was increased to  $0.33\text{ g/g } \gamma\text{-Al}_2\text{O}_3$  (curve e). The increase in KF loading might lead to catalyst saturation on  $\text{Al}_2\text{O}_3$ , thus, above the loading of  $0.24\text{ g/g } \gamma\text{-Al}_2\text{O}_3$  some of the catalyst might not interact with the support. This observation is consistent with the literature [20].

Fig. 4 shows the XRD patterns of the  $\text{NaNO}_3/\gamma\text{-Al}_2\text{O}_3$  catalyst calcined at  $500^\circ\text{C}$ . Only diffraction lines of  $\gamma\text{-Al}_2\text{O}_3$  (JCPDS File No. 00-029-0063) at  $2\theta = 45.79^\circ$  and  $66.76^\circ$  were visible in the case of  $0.06\text{ g/g } \gamma\text{-Al}_2\text{O}_3$  (curve a). At this loading, the  $\text{NaNO}_3$  phase could not be detected, probably due to the decomposition of  $\text{NaNO}_3$  during calcination process at  $500^\circ\text{C}$ . When the loading amount was increased to  $0.15\text{ g/g } \gamma\text{-Al}_2\text{O}_3$ , the formation of  $\text{NaAlO}_2$  (JCPDS File No. 00-019-1179) at  $2\theta = 30.38^\circ$  and  $\text{Na}_2\text{O}$  (JCPDS File No. 00-023-0528) at  $2\theta = 32.17^\circ$ , along with the  $\gamma\text{-Al}_2\text{O}_3$  phases, were noted (curve b). As the loading amount was increased to  $0.24$  and  $0.30\text{ g/g } \gamma\text{-Al}_2\text{O}_3$ , the relative intensity of the peak corresponding to the  $\text{NaAlO}_2$  phase was found to increase (curve c), indicating an increase in the degree of crystallinity of the phase. When the  $\text{NaNO}_3$  content was further increased to  $0.33\text{ g/g } \gamma\text{-Al}_2\text{O}_3$ , a strong diffraction peak attributed to  $\text{NaNO}_3$  (JCPDS File No. 00-006-0392) phase appeared at  $2\theta = 29.69^\circ$ , implying that the  $\text{NaNO}_3$  on  $\gamma\text{-Al}_2\text{O}_3$  support was over-saturated (curve e). This observation is in good agreement with the literature [6].

### 3.3. Basicity of the catalyst

The  $\text{CO}_2$ -TPD measurements were performed for an assessment of the total basicity and the basic site distributions on the catalyst. The TPD profiles of desorbed  $\text{CO}_2$  on  $\text{KF}/\gamma\text{-Al}_2\text{O}_3$  and  $\text{NaNO}_3/\gamma\text{-Al}_2\text{O}_3$  catalysts are shown in Figs. 5 and 6, respectively. Both catalysts showed complex desorption profiles, which could be due to the presence of a variety of basic sites of different strength. In

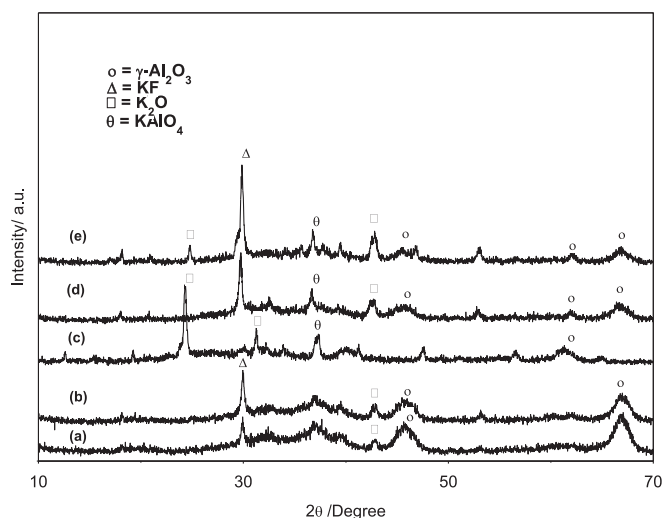


Fig. 3. XRD spectrum of  $\text{KF}/\gamma\text{-Al}_2\text{O}_3$  catalyst with different KF loadings (a)  $0.06\text{ g/g } \gamma\text{-Al}_2\text{O}_3$  (b)  $0.15\text{ g/g } \gamma\text{-Al}_2\text{O}_3$  (c)  $0.24\text{ g/g } \gamma\text{-Al}_2\text{O}_3$  (d)  $0.30\text{ g/g } \gamma\text{-Al}_2\text{O}_3$  (e)  $0.33\text{ g/g } \gamma\text{-Al}_2\text{O}_3$ .

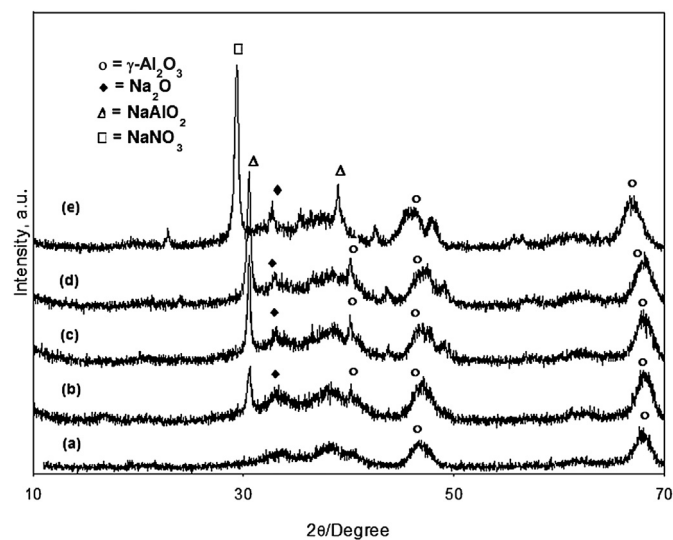
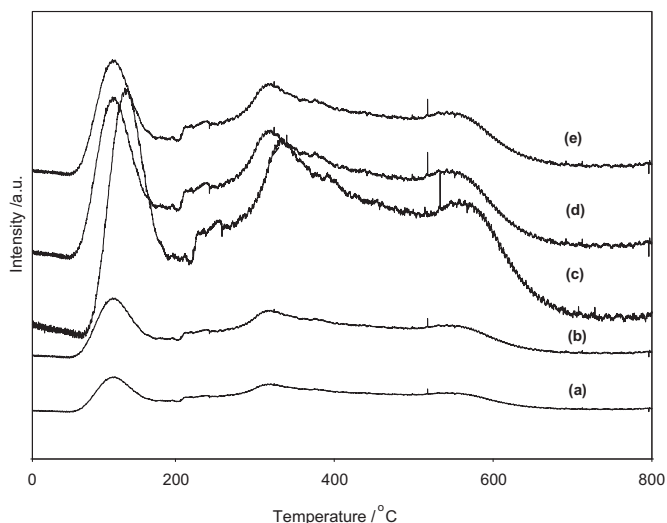


Fig. 4. XRD spectrum of  $\text{NaNO}_3/\gamma\text{-Al}_2\text{O}_3$  catalyst with different  $\text{NaNO}_3$  loadings: (a)  $0.06\text{ g/g } \gamma\text{-Al}_2\text{O}_3$  (b)  $0.15\text{ g/g } \gamma\text{-Al}_2\text{O}_3$  (c)  $0.24\text{ g/g } \gamma\text{-Al}_2\text{O}_3$  (d)  $0.30\text{ g/g } \gamma\text{-Al}_2\text{O}_3$  (e)  $0.33\text{ g/g } \gamma\text{-Al}_2\text{O}_3$ .



**Fig. 5.** CO<sub>2</sub>-TPD profiles of KF/γ-Al<sub>2</sub>O<sub>3</sub> catalyst with different KF loadings: (a) 0.06 g/g γ-Al<sub>2</sub>O<sub>3</sub> (b) 0.15 g/g γ-Al<sub>2</sub>O<sub>3</sub> (c) 0.24 g/g γ-Al<sub>2</sub>O<sub>3</sub> (d) 0.30 g/g γ-Al<sub>2</sub>O<sub>3</sub> (e) 0.33 g/g γ-Al<sub>2</sub>O<sub>3</sub>.

general, a higher temperature is needed to desorb the CO<sub>2</sub> adsorbed on the more strongly basic sites. The desorption peaks at 100 and 332 °C of KF/γ-Al<sub>2</sub>O<sub>3</sub> can be attributed to the interaction of CO<sub>2</sub> with weak and medium strength basic sites, respectively. In the case of NaNO<sub>3</sub>/γ-Al<sub>2</sub>O<sub>3</sub> (Fig. 6), the TPD profiles showed two weak peaks, one at 230 °C and another at 321 °C, which are characteristic of CO<sub>2</sub> desorption from medium–basic sites [21]. The desorption peaks at 576 °C for KF/γ-Al<sub>2</sub>O<sub>3</sub> and 525 °C for NaNO<sub>3</sub>/γ-Al<sub>2</sub>O<sub>3</sub> (Figs. 5 and 6) indicated basic sites of high strength, which are related to the presence of free O<sup>2-</sup> anions [22].

The numbers of total basic sites on the catalysts are summarized in Table 2. The basicity of the catalysts was found to affect by the catalyst loading. The basicity of catalysts increased with the KF or NaNO<sub>3</sub> loading until reaching a maximum value of 0.24 g/g γ-Al<sub>2</sub>O<sub>3</sub> for NaNO<sub>3</sub>/γ-Al<sub>2</sub>O<sub>3</sub> and 0.30 g/g γ-Al<sub>2</sub>O<sub>3</sub> for NaNO<sub>3</sub>/γ-Al<sub>2</sub>O<sub>3</sub>. Further increase in the loading of both catalysts was found to reduce the basicity. It was reported by Chorkendorff et al. [23] that the basic

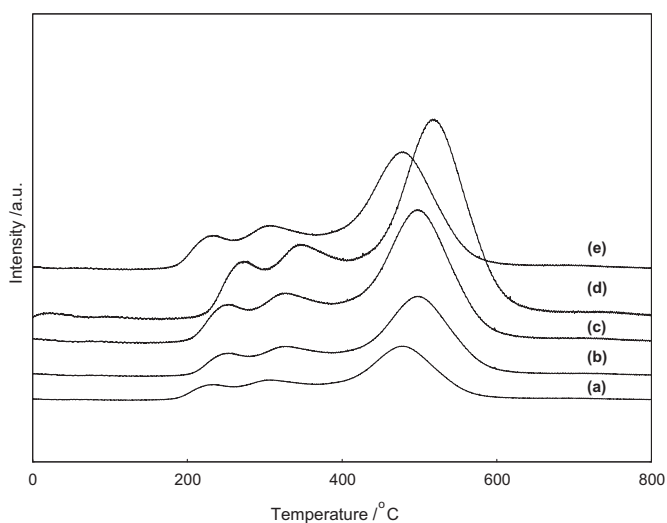


**Fig. 6.** CO<sub>2</sub>-TPD profiles of NaNO<sub>3</sub>/γ-Al<sub>2</sub>O<sub>3</sub> catalyst with different NaNO<sub>3</sub> loadings: (a) 0.06 g/g γ-Al<sub>2</sub>O<sub>3</sub> (b) 0.15 g/g γ-Al<sub>2</sub>O<sub>3</sub> (c) 0.24 g/g γ-Al<sub>2</sub>O<sub>3</sub> (d) 0.30 g/g γ-Al<sub>2</sub>O<sub>3</sub> (e) 0.33 g/g γ-Al<sub>2</sub>O<sub>3</sub>.

**Table 2**

CO<sub>2</sub>-TPD spectrum of millimetric γ-Al<sub>2</sub>O<sub>3</sub> particles with different catalyst loadings.

KF/γ-Al <sub>2</sub> O <sub>3</sub> catalyst		NaNO <sub>3</sub> /γ-Al <sub>2</sub> O <sub>3</sub> catalyst	
KF catalyst loading (g/g γ-Al <sub>2</sub> O <sub>3</sub> )	CO <sub>2</sub> desorbed (μmol/g catalyst)	NaNO <sub>3</sub> catalyst loading (g/g γ-Al <sub>2</sub> O <sub>3</sub> )	CO <sub>2</sub> desorbed (μmol/g catalyst)
0.06	304	0.06	408
0.15	505	0.15	509
0.24	703	0.24	690
0.30	611	0.30	760
0.33	604	0.33	700

sites of oxide phases can work synergetically with Lewis acid sites constituting acid–base pair sites which provide sufficient adsorptive sites for catalysis (see Fig. 7). The generation of active bases such as, K<sub>2</sub>O and KAlF<sub>4</sub> phases on KF/γ-Al<sub>2</sub>O<sub>3</sub> catalyst at 0.24 g/g γ-Al<sub>2</sub>O<sub>3</sub> as well as Na<sub>2</sub>O and NaAlO<sub>2</sub> phases on NaNO<sub>3</sub>/γ-Al<sub>2</sub>O<sub>3</sub> catalyst at 0.30 g/g γ-Al<sub>2</sub>O<sub>3</sub> might desorb higher amount of CO<sub>2</sub> and increase the basicity. The highest basicity was found to be 703 μmol/g catalyst and 759 μmol/g catalyst at a KF content of 0.24 g/g γ-Al<sub>2</sub>O<sub>3</sub> and NaNO<sub>3</sub> content of 0.30 g/g γ-Al<sub>2</sub>O<sub>3</sub>, respectively. The results also show that the catalyst basicity had strong influence on the catalytic activity in transesterification reaction where the highest biodiesel yields were obtained with catalysts of highest basicity (see Table 2 and Fig. 9).

At higher loading, the decrement in basicity for both catalysts was observed (see Table 2). These observations could be due to overloading of KF and NaNO<sub>3</sub> that saturated the Al<sub>2</sub>O<sub>3</sub> surface. As a result, the dispersion of excess KF and NaNO<sub>3</sub> could mask the active base sites which serve as active sites for transesterification reaction. Similar observations have been found by Taufiq-Yap et al. [20] and reported that a decrease in basicity at high catalyst loading was due to reduction of active bases in the structure of catalyst. The results showed that the basic sites as well as the basic strength of the supported catalysts were affected by the catalyst loading, which is in good agreement with the findings of other authors [24]. It is evident from the TPD profile that the NaNO<sub>3</sub>/γ-Al<sub>2</sub>O<sub>3</sub> catalyst (Fig. 6) showed more basic sites with a higher intensity of strongly basic sites compared with the KF/γ-Al<sub>2</sub>O<sub>3</sub> catalyst (Fig. 4).

#### 3.4. Surface area and pore structure of catalyst

Fig. 8 shows the nitrogen adsorption/desorption isotherms and pore size distributions of the catalysts. As shown in Fig. 8a, the isotherm of the γ-Al<sub>2</sub>O<sub>3</sub> support can be described as a type IV isotherm according to the IUPAC classifications. The isotherm displayed a steep hysteresis loop at relative pressures (*P*/*P*<sub>0</sub>) in the range between 0.8 and 1.0, and it showed a similar shape to those reported for mesoporous materials [25].

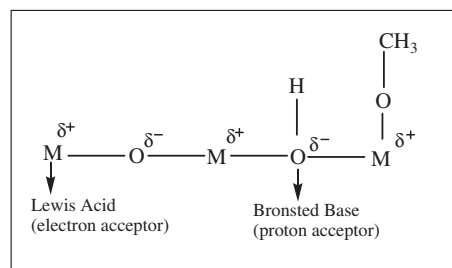


**Fig. 7.** Proposed mechanism of basic catalyst (formation of partial negative charge near the oxygen atom due to unshared pairs of electrons and partial positive charge near the metal atoms [23]).

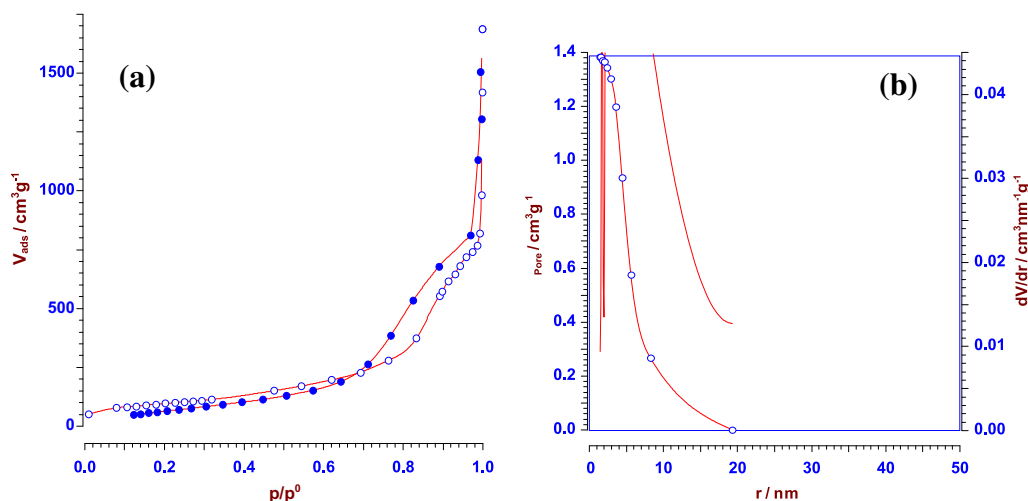


Fig. 8.  $N_2$  adsorption–desorption isotherm (a) and BJH pore size distribution (b) of the millimetric  $\gamma$ - $Al_2O_3$  particles.

The pore size distribution of the  $\gamma$ - $Al_2O_3$  support determined by the Barrett, Joyner and Halenda (BJH) method from the adsorption branch of the isotherm exhibited one single narrow peak (unimodal distribution) centered at 5.8–6.1 nm (Fig. 8b). The unimodal pore size distribution indicated the presence of monodisperse pores in the particles. Table 3 compiles the surface area, pore volume and pore diameter of the catalysts. As shown in Table 3, the  $\gamma$ - $Al_2O_3$  support gave a high surface area of 349  $m^2/g$ , indicating a high thermal stability of the sol–gel derived  $\gamma$ - $Al_2O_3$  support [26]. With an increase in KF content from 0.06 g to 0.33 g/g  $\gamma$ - $Al_2O_3$ , the surface area of the catalyst decreased from 319 to 143  $m^2/g$  (Table 3), along with a decrease in the pore volume and pore size. In the case of the  $NaNO_3/\gamma$ - $Al_2O_3$  catalyst, the surface area decreased from 322 to 152  $m^2/g$ , while the pore diameter decreased from 9.4 to 4.1 nm (Table 3). This gradual loss of surface area has been previously observed and attributed to the effect of catalyst deposition on the support, which resulted in partial blocking of the porous network [8,24].

### 3.5. Catalytic activity

The influence of catalyst loading on the FAME yield was investigated, as shown in Fig. 9. The yield was found to increase when the KF content was increased from 0.06 to 0.24 g/g  $\gamma$ - $Al_2O_3$ , with

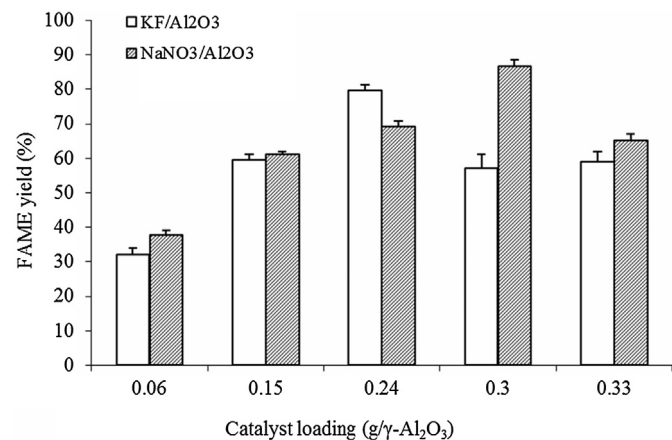


Fig. 9. Effect of KI and  $NaNO_3$  catalyst loadings on FAME yield. Reaction conditions: Methanol/oil molar ratio of 14:1, catalyst amount 0.6 g (4 wt%,  $g_{cat}/g_{oil}$ , calcined at 500 °C), reaction temperature of 60 °C, reaction time of 4 h.

the highest FAME yield of 80% obtained at a loading of 0.24 g/g  $\gamma$ - $Al_2O_3$ . On the other hand, the highest FAME yield obtained for the  $NaNO_3/\gamma$ - $Al_2O_3$  catalyst was 87% at a loading of 0.3 g/g  $\gamma$ - $Al_2O_3$ .

The metal oxide provides sufficient adsorptive sites for alcohol in transesterification reaction. Chorkendorff et al. [23] pointed out that the high transesterification activity of catalyst might be due to the manifestation of the dissociation of alcohol to  $RO^-$  and  $H^+$  on basic sites of metal oxide catalyst surface (Fig. 7). The methoxide ( $RO^-$ ) anions then react with triglyceride molecules to yield methyl esters. Thus, the high yield of biodiesel could be attributed to the generation of active phases such as,  $K_2O$ ,  $KAlF_4$  phases at 0.24 g/g  $\gamma$ - $Al_2O_3$  for the  $KF/\gamma$ - $Al_2O_3$  catalyst and  $Na_2O$ ,  $NaAlO_2$  phases at 0.30 g/g  $\gamma$ - $Al_2O_3$  for the  $NaNO_3/\gamma$ - $Al_2O_3$  catalyst. However, at higher loadings, i.e. above 0.24 g/g  $\gamma$ - $Al_2O_3$  for KF and above 0.30 g/g  $\gamma$ - $Al_2O_3$  for  $NaNO_3$ , the uptake of the catalysts might be saturated and thus, the decomposition of catalyst might be precluded, as evident from XRD. Therefore, the basicity as well as the catalyst activity might be reduced as evidenced by decreased basicity and catalytic activity (see Table 2, Fig. 9).

In addition, the biodiesel yield could also be affected by a difference in the number of basic sites as well as the level of strongly basic sites present in the catalysts. Since the ability of bases to abstract a proton from an alcohol is directly connected to the base strength, stronger bases are in general more effective to initiate the transesterification of triglycerides [23]. Thus, the formation of the oxide phase may contribute to higher basicity as well as catalytic activity towards the transesterification reaction. As per the TPD- $CO_2$  result, the higher level of basic sites and strength of the  $NaNO_3/\gamma$ - $Al_2O_3$  catalyst at a loading of 0.3 g/g  $\gamma$ - $Al_2O_3$  (see curve d in Fig. 6)

Table 3

BET surface area and pore structure of millimetric  $\gamma$ - $Al_2O_3$  particles with different catalyst loadings.

Catalyst type	Catalyst loading (g/g $\gamma$ - $Al_2O_3$ )	Pore volume ( $cm^3/g$ )	Surface area ( $m^2/g$ )	Pore diameter (nm)
$\gamma$ - $Al_2O_3$	—	1.38	349	11.2
KF/ $\gamma$ - $Al_2O_3$	0.06	1.21	319	9.3
	0.15	0.92	291	7.5
	0.24	0.85	265	6.9
	0.30	0.65	199	5.7
	0.33	0.53	143	3.9
$NaNO_3/\gamma$ - $Al_2O_3$	0.06	1.19	322	9.4
	0.15	0.97	304	7.3
	0.24	0.83	287	6.2
	0.30	0.65	203	5.1
	0.33	0.49	152	4.1

might result in a higher biodiesel yield compared with the KF/ $\gamma$ -Al<sub>2</sub>O<sub>3</sub> catalyst (see curve c in Fig. 5). Although both impregnated catalysts exhibited a decrease in surface area, pore diameter and pore volume at higher loadings, their pore structures were found to be that of mesopores (i.e., >2 nm in diameter) (Table 3). It has been proposed that mesoporous catalysts permit the diffusion of large molecules like triglycerols into the active sites, thereby promoting the transesterification reaction [25]. At lower catalyst loading, the catalyst activity was found to be strongly dependent on the catalyst basicity whereas at higher catalyst loading, the catalyst activity could be affected by the surface area of the catalyst. For example, the catalytic activity of KF catalyst with higher loading of 0.33 g/g  $\gamma$ -Al<sub>2</sub>O<sub>3</sub> compared to 0.15 g/g  $\gamma$ -Al<sub>2</sub>O<sub>3</sub> was found to be lower, although the former had higher basicity. This phenomenon might be due to the lower catalyst surface area at higher loading that offset the benefit of higher basicity. The surface area of catalyst with loading of 0.33 g/g  $\gamma$ -Al<sub>2</sub>O<sub>3</sub> was about halved of that of 0.15 g/g  $\gamma$ -Al<sub>2</sub>O<sub>3</sub> for both catalysts (see Table 3). Similar results have also been reported by Taufiq-Yap et al. [20].

More importantly, the biodiesel yields obtained using the macrocatalysts prepared in this study was significantly higher than that of the macrocatalysts used by Wang et al. [12]. In addition, it was reported that the activity of powdered alumina supported catalysts such as KI, KF, HNO<sub>3</sub>, K<sub>2</sub>CO<sub>3</sub>, NaNO<sub>3</sub>, or KOH was reduced after successive reuse due to the leaching of active species during reaction [2,3,6,18,27]. It would be interesting to determine whether the use of millimetric size support could improve the catalyst reusability and this forms the basis for future study.

#### 4. Conclusions

The use of spherical millimetric  $\gamma$ -Al<sub>2</sub>O<sub>3</sub> support particles loaded with KF or NaNO<sub>3</sub> catalysts for the transesterification of palm oil and methanol to biodiesel was demonstrated. The biodiesel yield could be attributed to the formation of new phases, the presence of basic sites and the strength of the sites, as well as the surface area and mesoporous structure of the support. The biodiesel yield was comparable to that produced from smaller catalysts, which indicates the potential of the macrospherical catalysts.

#### References

- [1] Zabeti M, Wan-Daud WMA, Aroua MK. Activity of solid catalysts for biodiesel production: a review. *Fuel Processing Technology* 2009;90:770–7.
- [2] Xie W, Li H. Alumina-supported potassium iodide as a heterogeneous catalyst for biodiesel production from soybean oil. *Journal of Molecular Catalysis A: Chemical* 2006;255:1–9.
- [3] Benjapornkulaphong S, Ngamcharussrivichai C, Bunyakiat K. Al<sub>2</sub>O<sub>3</sub>-supported alkali and alkali earth metal oxides for transesterification of palm kernel oil and coconut oil. *Chemical Engineering Journal* 2009;145:468–74.
- [4] Kim HJ, Kang BS, Kim MJ, Park YM, Kim DK, Lee JS, et al. Transesterification of vegetable oil to biodiesel using heterogeneous base catalyst. *Catalysis Today* 2004;93–95:315–20.
- [5] Arzamendi G, Campoa I, Arguinarena E, Sanchez M, Montes M, Gandia LM. Synthesis of biodiesel with heterogeneous NaOH/alumina catalysts: comparison with homogeneous NaOH. *Chemical Engineering Journal* 2007;134:123–30.
- [6] Xie W, Peng H, Chen L. Transesterification of soybean oil catalyzed by potassium loaded on alumina as a solid-base catalyst. *Applied Catalysis A: General* 2006;300:67–74.
- [7] Ma H, Li S, Wang B, Wang R, Tian S. Transesterification of rapeseed oil for synthesizing biodiesel by K/KOH/ $\gamma$ -Al<sub>2</sub>O<sub>3</sub> as heterogeneous base catalyst. *Journal of the American Oil Chemists Society* 2008;85:263–70.
- [8] Boz N, Degirmenbasi N, Kalyon DM. Conversion of biomass to fuel: transesterification of vegetable oil to biodiesel using KF loaded nano- $\gamma$ -Al<sub>2</sub>O<sub>3</sub> as catalyst. *Applied Catalysis B: Environmental* 2009;89:590–6.
- [9] Han H, Guan Y. Synthesis of biodiesel from rapeseed oil using K<sub>2</sub>O/ $\gamma$ -Al<sub>2</sub>O<sub>3</sub> as nano-solid-base catalyst. *Journal of Natural Sciences* 2009;14:75–9.
- [10] Centi G, Perathoner S. Novel catalyst design for multiphase reactions. *Catalysis Today* 2003;79–80:3–13.
- [11] Matatov-Meytal Y, Sheintuch M. Catalytic fibers and cloths. *Applied Catalysis A: General* 2002;231:1–16.
- [12] Wang Y, Zhang F, Xu S, Yang L, Li D, Evans DG, et al. Preparation of macrospherical magnesia-rich magnesium aluminate spinel catalysts for methanolysis of soybean oil. *Chemical Engineering Science* 2008;63:4306–12.
- [13] Campanati M, Fornasari G, Vaccari A. Fundamentals in the preparation of heterogeneous catalysts. *Catalysis Today* 2003;77:299–314.
- [14] Wang ZM, Lin YS. Sol-gel synthesis of pure and copper oxide coated mesoporous alumina granular particles. *Journal of Catalysis* 1998;174:43–51.
- [15] Chan ES. Preparation of Ca-alginate beads containing high oil content: influence of process variables on encapsulation efficiency and bead properties. *Carbohydrate Polymers* 2011;84(4):1267–75.
- [16] Akbar E, Binit N, Yaako Z, Kamarudin SK, Salimon J. Preparation of Na doped SiO<sub>2</sub> solid catalysts by the sol-gel method for the production of biodiesel from jatropha oil. *Green Chemistry* 2009;11:1862–6.
- [17] Encinar JM, Gonzalez JF, Rodriguez-Reinares A. Biodiesel from used frying oil. Variables affecting the yields and characteristics of the biodiesel. *Industrial and Engineering Chemistry Research* 2005;44:5491–9.
- [18] Alonso DM, Mariscal R, Tost RM, Poves MDZ, Lopez M. Potassium leaching during triglyceride transesterification using K/ $\gamma$ -Al<sub>2</sub>O<sub>3</sub> catalysts. *Catalysis Communications* 2007;8:2074–80.
- [19] Chan ES, Lee BB, Ravindra P, Poncelet D. Shape and size analysis of Ca-alginate particles produced through extrusion-dripping method. *Journal of Colloid and Interface Science* 2009;338:63–72.
- [20] Taufiq-Yap YH, Lee HV, Yunus R, Juan JC. Transesterification of non-edible Jatropha curcas oil to biodiesel using binary Ca–Mg mixed oxide catalyst: effect of stoichiometric composition. *Chemical Engineering Journal* 2011;178:342–7.
- [21] Bolognini M, Cavani F, Scagliarini D, Flego C, Perego C, Saba M. Heterogeneous basic catalysts as alternatives to homogeneous catalysts: reactivity of Mg/Al mixed oxides in the alkylation of m-cresol with methanol. *Catalysis Today* 2002;75:103–11.
- [22] Serio MD, Ledda M, Cozzolino M, Minutillo G, Tesser R, Santacesaria E. Transesterification of soybean oil to biodiesel by using heterogeneous basic catalysts. *Industrial and Engineering Chemistry Research* 2006;45:3009–14.
- [23] Chorkendorff I, Niemantsverdriet JW. Concepts of modern catalysis and kinetics. Germany: Wiley-VCH Weinheim; 2003.
- [24] Meher LC, Kulkarni MG, Dalai AK, Naik SN. Transesterification of karanja (*Pongamia pinnata*) oil by solid basic catalysts. *European Journal of Lipid Science and Technology* 2006;108:389–97.
- [25] Melero JA, Stucky GD, Van Grieken R, Morales G. Direct syntheses of ordered SBA-15 mesoporous materials containing arenosulfonic acid groups. *Journal of Materials Chemistry* 2002;12:1664–70.
- [26] Cao JL, Wang Y, Zhang TY, Wu SH, Yuan ZY. Preparation, characterization and catalytic behavior of nanostructured mesoporous CuO/CeO<sub>2</sub>ZrO<sub>2</sub> catalysts for low-temperature CO oxidation. *Applied Catalysis B: Environmental* 2008;78:120–8.
- [27] Verziu M, Florea M, Simon S, Simon V, Filip P, Parvulescu VI, et al. Transesterification of vegetable oils on basic large mesoporous alumina supported alkaline fluorides—evidences of the nature of the active site and catalytic performances. *Journal of Catalysis* 2009;263:56–66.